# Large eddy simulation models for incompressible magnetohydrodynamics derived from the variational multiscale formulation

David Sondak and Assad A. Oberai

Citation: Phys. Plasmas **19**, 102308 (2012); doi: 10.1063/1.4759157
View online: http://dx.doi.org/10.1063/1.4759157
View Table of Contents: http://pop.aip.org/resource/1/PHPAEN/v19/i10
Published by the American Institute of Physics.

# Large eddy simulation models for incompressible magnetohydrodynamics derived from the variational multiscale formulation

David Sondak[a] and Assad A. Oberai
*Rensselaer Polytechnic Institute, SCOREC, CII 4225, 110 8th Street, Troy, New York 12180, USA*

(Received 18 June 2012; accepted 2 October 2012; published online 24 October 2012)

Novel large eddy simulation (LES) models are developed for incompressible magnetohydrodynamics (MHD). These models include the application of the variational multiscale formulation of LES to the equations of incompressible MHD. Additionally, a new residual-based eddy viscosity model is introduced for MHD. A mixed LES model that combines the strengths of both of these models is also derived. The new models result in a consistent numerical method that is relatively simple to implement. The need for a dynamic procedure in determining model coefficients is no longer required. The new LES models are tested on a decaying Taylor-Green vortex generalized to MHD and benchmarked against classical LES turbulence models. The LES simulations are run in a periodic box of size $[-\pi, \pi]^3$ with 32 modes in each direction and are compared to a direct numerical simulation (DNS) with 512 modes in each direction. The new models are able to account for the essential MHD physics which is demonstrated via comparisons of energy spectra. We also compare the performance of our models to a DNS simulation by Pouquet *et al.* ["The dynamics of unforced turbulence at high Reynolds number for Taylor–Green vortices generalized to MHD," Geophys. Astrophys. Fluid Dyn. **104**, 115–134 (2010)], for which the ratio of DNS modes to LES modes is 262:144. © *2012 American Institute of Physics*. [http://dx.doi.org/10.1063/1.4759157]

## I. INTRODUCTION

Incompressible magnetohydrodynamics (MHD) has various applications in the study of phenomena in our universe for both scientific exploration and engineering pursuits. Among these are the geodynamo theory and the origin of planetary magnetic fields, turbulence in the solar wind, fusion plasmas in tokamak reactors, and liquid metal studies in metallurgy.[1–5] It is very often the case that these systems are in a state of turbulence. Studying turbulent phenomena is difficult due to a lack of a theory on hydrodynamic turbulence, let alone MHD turbulence, and is compounded by the mathematical difficulties associated with the equations of MHD. These equations are a system of nonlinear partial differential equations consisting of the momentum equation for the velocity field augmented by the Lorentz force and Maxwell's equations. Combining Maxwell's equations results in a nonlinear equation for the magnetic induction. Because of the mathematical intractability of these equations and a dearth of experimental opportunities for most plasma systems, scientists often resort to numerical simulations to probe MHD phenomena.

There are, however, considerable difficulties in the numerical simulation of plasma systems. In particular, simply directly solving the incompressible MHD equations (direct numerical simulation or DNS) is not feasible even with today's computational resources. In fact, DNS of many interesting phenomena will remain elusive for the foreseeable future. One method for enabling realistic numerical simulations is to develop mathematical models that account for the information that is missing from a numerical simulation. Large eddy simulation (LES) involves directly simulating the largest scales in the flow-field while mathematically modeling scales smaller than the smallest resolved scale. Considerable work has been done pertaining to LES models for the hydrodynamic case, but less so for MHD.

Eddy viscosity models (EVMs) have been proposed for MHD by generalizing those for the hydrodynamic case.[6] These models are a good starting point, but do not account for significant portions of the subgrid physics. For example, they do not allow for the possibility of backscatter or a subgrid dynamo effect wherein turbulent velocity fluctuations transfer energy to the resolved magnetic induction. Furthermore, it has been shown that the dynamic Smagorinsky EVM (DSEVM) excessively damps out the effects of the dynamo effect in MHD.[7] Closures for the mean-field equations of MHD have been systematically worked out,[8] but these models are difficult to implement numerically. Newer models account for the coupled nature of the equations, permit the possibility of backscatter,[9] and are relatively straightforward to implement. These models depend on parameters that generally depend upon the flow field. Such parameters are determined on the fly during the computation with a dynamic procedure.[10] The dynamic procedure for determining the model coefficients is cumbersome to implement. In recent years, new eddy viscosity models have been proposed[11,12] that aim to eliminate the need for a dynamic procedure in the context of hydrodynamic turbulence. Other studies have dealt with LES for MHD in recent years. Work has been done for flows in which the magnetic Reynolds number is small compared to the hydrodynamic Reynolds number. One approach performs a DNS of the induction equation while using a subgrid LES model to represent the velocity field components that are smaller than the magnetic

[a]Electronic mail: sondad@rpi.edu.

 

diffusion length.[13] In yet another approach, the quasistatic approximation is used wherein the nonlinear terms in the magnetic induction equation are neglected.[14] Two point closure models in spectral space such as the eddy damped quasi normal Markovian (EDQNM) approximation[15] have been generalized[16] and applied to MHD.[17] Another popular closure model, the Lagrangian-averaged alpha model, introduces closure not through the diffusion terms but via the nonlinear terms.[18–20] This technique has also been applied to the MHD equations.[21]

Previous studies have been performed which apply stabilized finite elements to incompressible magnetohydrodynamics.[22,23] Although useful in overcoming spurious oscillations in the solution and circumventing the Ladyženskaja-Babuška-Brezzi condition,[24] stabilized finite elements only represent incomplete turbulence models. In this work, we develop novel LES turbulence models for incompressible MHD that are derived from the variational multiscale (VMS) formulation.[25] These models are able to account for much of the desired physics in incompressible MHD turbulence and do not rely on a dynamic procedure. Further, they automatically vanish when the coarse resolved scales are close to the "exact solution" of the MHD equations.

The layout of the remainder of this manuscript is as follows. In Sec. II, the incompressible MHD equations and their variational counterpart are discussed. This section also discusses the concept of scale separation and its implications for numerical methods. In Sec. III, an overview of a subset of existing LES models is given and the new models are presented. The following models are considered in this work: the DSEVM, a model based on the residual-based VMS formulation, a new residual-based eddy viscosity model (RBEVM), and a new mixed model (MM) that combines the VMS and the RBEVM. In Sec. IV, we present the results in predicting a Taylor-Green flow generalized to MHD, and in Sec. V, we draw conclusions and discuss future work. From the models proposed and tested in this manuscript, we conclude that the mixed model is the most comprehensive and accurate.

## II. PHYSICAL AND NUMERICAL BACKGROUND

### A. Equations of incompressible MHD

The single-fluid incompressible MHD equations are

$$\frac{\partial \mathbf{u}}{\partial t} + \nabla \cdot (\mathbf{u} \otimes \mathbf{u}) - \nabla \cdot (\mathbf{B} \otimes \mathbf{B}) + \nabla P - \nu \nabla^2 \mathbf{u} = \mathbf{f}, \quad (1)$$

$$\nabla \cdot \mathbf{u} = 0, \quad (2)$$

$$\frac{\partial \mathbf{B}}{\partial t} - \nabla \cdot (\mathbf{u} \otimes \mathbf{B}) + \nabla \cdot (\mathbf{B} \otimes \mathbf{u}) + \nabla r - \eta \nabla^2 \mathbf{B} = \mathbf{g}, \quad (3)$$

$$\nabla \cdot \mathbf{B} = 0. \quad (4)$$

Equation (1) is the momentum equation for the velocity field $\mathbf{u}$ along with the solenoidal constraint on the velocity field (Eq. (2)) which ensures incompressibility. The field $P$ is the pressure field. It is related to the fluid pressure, $p_f$, via $P = p_f/\rho + \mathbf{B} \cdot \mathbf{B}/2$. The kinematic viscosity of the fluid with density $\rho$ is denoted by $\nu$. Equation (3) is the induction equation for the magnetic induction $\mathbf{B}$. The induction equation is accompanied by the solenoidal constraint on the magnetic induction which says that there are no magnetic monopoles (Eq. (4)). The magnetic diffusivity is given by $\eta = 1/(\mu\sigma)$, where $\mu$ is the magnetic permeability and $\sigma$ is the electrical conductivity of the fluid. We have also included an artificial magnetic pressure $r$ in the induction equation which acts as a Lagrange multiplier that enforces the divergence free constraint on the magnetic induction. This artificial magnetic pressure is useful when working within a finite element context to help to numerically enforce the divergence free constraint on the magnetic induction. In the realm of spectral methods, an additional benefit is that the pressures can be eliminated analytically. Therefore, it is only necessary to numerically solve for the two vector fields. If one desires, the pressures can be recovered as part of a post-processing step. In the equations above, the magnetic induction has been rescaled to be in Alfvén velocity units. Both Eqs. (1) and (3) also include the possibility of volumetric forces $\mathbf{f}$ and $\mathbf{g}$.

In the remainder of the paper, Eqs. (1)–(4) will be written as

$$\frac{\partial \mathbf{u}}{\partial t} + \nabla \cdot \boldsymbol{\mathcal{N}}_V + \nabla P - \nu \nabla^2 \mathbf{u} = \mathbf{f}, \quad (5)$$

$$\nabla \cdot \mathbf{u} = 0, \quad (6)$$

$$\frac{\partial \mathbf{B}}{\partial t} + \nabla \cdot \boldsymbol{\mathcal{N}}_I + \nabla r - \eta \nabla^2 \mathbf{B} = \mathbf{g}, \quad (7)$$

$$\nabla \cdot \mathbf{B} = 0, \quad (8)$$

in which the nonlinear terms are written as

$$\boldsymbol{\mathcal{N}}_V(\mathbf{U}) = \mathbf{u} \otimes \mathbf{u} - \mathbf{B} \otimes \mathbf{B} \quad (9)$$

for the momentum equation and

$$\boldsymbol{\mathcal{N}}_I(\mathbf{U}) = -\mathbf{u} \otimes \mathbf{B} + \mathbf{B} \otimes \mathbf{u} \quad (10)$$

for the induction equation, where $\mathbf{U} = [\mathbf{u}, P, \mathbf{B}, r]^T$ is a vector of the solution fields.

This system of equations is completed with appropriate boundary conditions. In this work, we use $2\pi-$ periodic boundary conditions for $\mathbf{u}$, $\mathbf{B}$, $P$, and $r$. The numerical method we use is therefore a Fourier-spectral method.

### B. Variational formulation

The equivalent variational statement to Eqs. (5)–(8) is: Find $\mathbf{U} \in \boldsymbol{\mathcal{V}}$ such that $\forall\, \mathbf{W} \in \boldsymbol{\mathcal{V}}$,

$$\mathcal{A}(\mathbf{W}, \mathbf{U}) = (\mathbf{W}, \mathbf{F}). \quad (11)$$

In Eq. (11), $\mathbf{W} = [\mathbf{w}, q, \mathbf{v}, s]^T$ is a vector of weighting functions and $\mathbf{U} = [\mathbf{u}, P, \mathbf{B}, r]^T$ is a vector of trial solutions. $\mathbf{F} = [\mathbf{f}, 0, \mathbf{g}, 0]^T$ is a vector of forcing functions. The goal is to determine $\mathbf{U}$. The weighting functions and trial solutions reside in a function space denoted by $\boldsymbol{\mathcal{V}}$. This space is equipped with functions that have the desired smoothness

properties and boundary conditions. Before defining the space $\mathcal{V}$, we first introduce some notation. The $L_2$ inner product in a domain $\Omega$ for a vector function $\mathbf{h}$ is

$$(\mathbf{h},\mathbf{h}) = \int_\Omega \mathbf{h}\cdot\mathbf{h}\, d\Omega. \tag{12}$$

The corresponding $L_2$ norm is

$$\|\mathbf{h}\|_{L_2} = \sqrt{(\mathbf{h},\mathbf{h})}. \tag{13}$$

The $H^1$ inner product is

$$(\mathbf{h},\mathbf{h})_{H^1} = \int_\Omega (\mathbf{h}\cdot\mathbf{h} + \nabla\mathbf{h} : \nabla\mathbf{h})\, d\Omega. \tag{14}$$

The corresponding $H^1$ norm is

$$\|\mathbf{h}\|_{H^1} = \sqrt{(\mathbf{h},\mathbf{h})_{H^1}}. \tag{15}$$

The function space $\mathcal{V}$ is defined as

$$\begin{aligned}\mathcal{V} \equiv \{\mathbf{W}\,|\,\mathbf{W} = [\mathbf{w},\, q,\, \mathbf{v},\, s]^T,\\ \mathbf{w},\, \mathbf{v} \in H^1(\Omega), q,\, s \in L_2(\Omega),\\ \mathbf{W}(\mathbf{y},t) = \mathbf{W}(\mathbf{x},t)\}\end{aligned} \tag{16}$$

in a cubic domain $\Omega$ with boundary $\partial\Omega$. Each of the six faces of the cube $\Gamma_j(-\pi)$, $\Gamma_j(\pi), j = 1,2,3$ are given by

$$\Gamma_j(c) = \{\mathbf{x}\in\partial\Omega\,|\,\mathbf{x}_j = c\}, \tag{17}$$

so that

$$\mathbf{y} = \mathbf{x} + 2\pi\mathbf{e}_j \in \Gamma_j(\pi), \tag{18}$$

where $\mathbf{e}_j$ is the unit Cartesian vector in the $\mathbf{x}_j$ direction. The space $L_2(\Omega)$ is defined as

$$L_2(\Omega) = \{\mathbf{h}\in\Omega\,|\,\|\mathbf{h}\|_{L_2} < \infty\}. \tag{19}$$

This means that the pressures are bounded for all time. Similarly, the space $H^1(\Omega)$ is defined as

$$H^1(\Omega) = \{\mathbf{h}\in\Omega\,|\,\|\mathbf{h}\|_{H^1} < \infty\}. \tag{20}$$

This implies that the velocity and magnetic induction, as well as their first derivatives, remain bounded for all time. We are now ready to define the semi-linear form $\mathcal{A}(\mathbf{W},\mathbf{U})$,

$$\begin{aligned}\mathcal{A}(\mathbf{W},\mathbf{U}) = {}&(\mathbf{w},\mathbf{u}_{,t}) + (\mathbf{w},\nabla\cdot\boldsymbol{\mathcal{N}}_V) + (\mathbf{w},\nabla P) + (\nabla^s\mathbf{w}, 2\nu\nabla^s\mathbf{u})\\ &+ (q,\nabla\cdot\mathbf{u}) + (\mathbf{v},\mathbf{B}_{,t}) + (\mathbf{v},\nabla\cdot\boldsymbol{\mathcal{N}}_I) + (\mathbf{v},\nabla r)\\ &+ (\nabla^s\mathbf{v}, 2\eta\nabla^s\mathbf{B}) + (s,\nabla\cdot\mathbf{B}).\end{aligned} \tag{21}$$

In the equation above, $\nabla^s$ is the symmetric gradient operator defined as $\nabla^s\mathbf{h} \equiv (\nabla\mathbf{h} + (\nabla\mathbf{h})^T)/2$. Due to periodic boundary conditions, no boundary terms appear in the semi-linear form.

Numerical methods rely on a discrete version of Eq. (11). The most straight-forward discretization is the Galerkin method. We introduce a conforming subspace of finite-dimensional functions as $\mathcal{V}^h \subset \mathcal{V}$. The mesh parameter $h$ represents the spacing of the grid points. The Galerkin method is: *Find* $\mathbf{U}^h \in \mathcal{V}^h$ *such that* $\forall\, \mathbf{W}^h \in \mathcal{V}^h$,

$$\mathcal{A}(\mathbf{W}^h,\mathbf{U}^h) = (\mathbf{W}^h,\mathbf{F}). \tag{22}$$

It is well-known that the Galerkin method does not provide accurate results for many problems. In particular, problems that involve many different scales such as turbulent flows or boundary layer flows, where $\mathcal{V}^h$ cannot represent all of the scales of the solution, are especially challenging. Next, we introduce the idea of scale separation.

### C. Scale separation

One reason why the Galerkin method is not able to produce high-fidelity results for all flow fields is because it does not account for all the necessary physics of the problem. In particular, it is not able to capture the physics of scales smaller than the mesh size. Let $\mathbf{U}$ be the "exact" solution to our problem. We define an optimal solution that lives in the finite dimensional space (the coarse-scale solution) through a projection operator $\mathbb{P}^h$. That is,

$$\mathbf{U}^h = \mathbb{P}^h\mathbf{U} \in \mathcal{V}^h. \tag{23}$$

Optimality is defined by the choice of the projection operator $\mathbb{P}^h$. Corresponding to the choice for the coarse-scale solution, there is a fine-scale solution defined as

$$\mathbf{U}' = \mathbf{U} - \mathbf{U}^h, \tag{24}$$

$$= (\mathbb{I} - \mathbb{P}^h)\mathbf{U}, \tag{25}$$

$$= \mathbb{P}'\mathbf{U} \in \mathcal{V}', \tag{26}$$

where $\mathbb{P}'$ is the fine-scale projection operator. With this, for any $\mathbf{U}\in\mathcal{V}$, we may uniquely define

$$\mathbf{U} = \mathbf{U}^h + \mathbf{U}'. \tag{27}$$

This leads to the decomposition of $\mathcal{V}$ into coarse- and fine-scale components

$$\mathcal{V} = \mathcal{V}^h + \mathcal{V}'. \tag{28}$$

We note that the same decomposition may be applied to the weighting functions as well,

$$\mathbf{W} = \mathbf{W}^h + \mathbf{W}'. \tag{29}$$

Using Eqs. (27) and (29) in the variational form (Eq. (11)) leads to two coupled equations: one for the resolved scales and one for the unresolved scales

$$\mathcal{A}(\mathbf{W}^h,\mathbf{U}^h + \mathbf{U}') = (\mathbf{W}^h,\mathbf{F}), \quad \forall\,\mathbf{W}^h \in \mathcal{V}^h, \tag{30}$$

$$\mathcal{A}(\mathbf{W}',\mathbf{U}^h + \mathbf{U}') = (\mathbf{W}',\mathbf{F}), \quad \forall\,\mathbf{W}' \in \mathcal{V}'. \tag{31}$$

This procedure is the starting point of the VMS formulation.[25] Equation (30) is the equation that is to be solved for

the coarse-scale solution $\mathbf{U}^h$. It differs from the Galerkin formulation in one important respect: the Galerkin formulation does not contain $\mathbf{U}'$. This is a very important difference and leads naturally to a discussion of LES. The aim of LES is to mathematically model the effects of $\mathbf{U}'$ on $\mathbf{U}^h$. We see that from Eq. (31) one may solve for $\mathbf{U}'$; indeed, this is precisely the next step in the VMS. Assuming that this equation can be solved (approximately), we can write the fine scales, $\mathbf{U}'$, as a functional of the coarse scales, and substituting this back in Eq. (30), we can devise new LES models. This is described in Sec. III A in the context of MHD.

Most other LES models are represented in a slightly different form. The effect of the fine scales on the coarse scales is modeled by appending a model term to the original Galerkin statement. That is, *find* $\mathbf{U}^h \in \mathcal{V}^h$ *such that* $\forall\, \mathbf{W}^h \in \mathcal{V}^h$,

$$\mathcal{A}(\mathbf{W}^h, \mathbf{U}^h) + \mathcal{M}(\mathbf{W}^h, \mathbf{U}^h; \mathbf{c}, h) = (\mathbf{W}^h, \mathbf{F}), \tag{32}$$

where the model term $\mathcal{M}(\cdot, \cdot; \cdot, \cdot)$ seeks to model the effects of $\mathbf{U}'$. It depends on the resolved-scale solution and is parameterized by some model parameters $\mathbf{c}$ and the mesh parameter $h$. Various specifications for $\mathcal{M}(\cdot, \cdot; \cdot, \cdot)$ are discussed in Sec. III.

*Remark:* For the Fourier-spectral functions we are working with, the projection operators are specifically chosen to be

$$\mathbb{P}^h \mathbf{U}(\mathbf{x}, t) = \sum_{|\mathbf{k}|_\infty \leq k^h} \hat{\mathbf{U}}(\mathbf{k}, t) e^{i\mathbf{k}\cdot\mathbf{x}}, \tag{33}$$

$$\mathbb{P}' \mathbf{U}(\mathbf{x}, t) = \sum_{|\mathbf{k}|_\infty > k^h} \hat{\mathbf{U}}(\mathbf{k}, t) e^{i\mathbf{k}\cdot\mathbf{x}}, \tag{34}$$

where $\hat{\mathbf{U}}(\mathbf{k}, t)$ represents the Fourier coefficients at wavenumber $\mathbf{k} = [k_1, k_2, k_3]^T$ and $|\mathbf{k}|_\infty = \max\{|k_1|, |k_2|, |k_3|\}$ with $k^h$ the cutoff wavenumber at $\pi/h$.

## III. OVERVIEW OF LES MODELS

In this section, we consider various LES models for incompressible MHD. The presentation of these models is as follows:

- We first briefly review the traditional Smagorinsky-type EVM in the context of incompressible MHD.
- Following this, we turn to the VMS formulation and apply it to incompressible MHD. The result is one type of LES model which is not an EVM.
- We then return to EVMs and introduce a new EVM that is motivated by an expression for the turbulent velocity fluctuations derived using the VMS formulation.
- Finally, we discuss a new mixed model that combines the VMS model with the new VMS-based EVM.

EVMs for incompressible MHD have the form

$$\mathcal{M}(\mathbf{W}^h, \mathbf{U}^h; \mathbf{c}, h) = (\nabla \mathbf{w}^h, 2\nu_T \nabla^s \mathbf{u}^h) + (\nabla \mathbf{v}^h, 2\eta_T \mathbf{J}^h). \tag{35}$$

The traditional Smagorinsky eddy viscosity model takes the eddy viscosity to be

$$\nu_T = (C_V^S h)^2 \mathcal{S}, \quad \mathcal{S} = \sqrt{2\nabla^s \mathbf{u}^h : \nabla^s \mathbf{u}^h}, \tag{36}$$

and the magnetic diffusivity to be[6]

$$\eta_T = (C_I^S h)^2 |\mathbf{j}^h|, \quad \mathbf{j}^h = \nabla \times \mathbf{B}^h. \tag{37}$$

In Eq. (35), $\mathbf{J}^h = \left(\nabla \mathbf{B}^h - (\nabla \mathbf{B}^h)^T\right)/2$ is the rate of rotation tensor for the magnetic induction. In Eqs. (36) and (37), $\mathcal{S}$ is a characteristic rate of strain and $\mathbf{j}^h$ is the current density. Further, $C_V^S$ and $C_I^S$ are coefficients that are determined via a dynamic procedure.[10]

### A. VMS

Applying the multiscale decomposition introduced in Sec. II C to the equations of incompressible MHD results in the problem (see Eq. (30)): *Find* $\mathbf{U}^h \in \mathcal{V}^h$ *such that* $\forall\, \mathbf{W}^h \in \mathcal{V}^h$,

$$\mathcal{A}(\mathbf{W}^h, \mathbf{U}^h + \mathbf{U}') = (\mathbf{W}^h, \mathbf{F}), \tag{38}$$

where

$$\begin{aligned}\mathcal{A}(\mathbf{W}^h, \mathbf{U}^h + \mathbf{U}') = \mathcal{A}(\mathbf{W}^h, \mathbf{U}^h) \\ + (\mathbf{w}^h, \nabla \cdot \boldsymbol{\mathcal{N}}_V^C) + (\mathbf{w}^h, \nabla \cdot \boldsymbol{\mathcal{N}}_V^R) \\ + (\mathbf{v}^h, \nabla \cdot \boldsymbol{\mathcal{N}}_I^C) + (\mathbf{v}^h, \nabla \cdot \boldsymbol{\mathcal{N}}_I^R).\end{aligned} \tag{39}$$

Note that all the terms in $\mathcal{A}(\mathbf{W}^h, \mathbf{U}^h + \mathbf{U}')$ that are linear in $\mathbf{U}'$ evaluate to zero because of the orthogonality of the functions in $\mathcal{V}^h$ and $\mathcal{V}'$. Further, in Eq. (39), a superscript $C$ represents cross stress terms (interactions between subgrid and resolved solutions) and a superscript $R$ represents the Reynolds stress terms (interactions solely between subgrid solutions). In particular,

$$\begin{aligned}\boldsymbol{\mathcal{N}}_V^C &= (\mathbf{u}^h \otimes \mathbf{u}' + \mathbf{u}' \otimes \mathbf{u}^h) \\ &\quad -(\mathbf{B}^h \otimes \mathbf{B}' + \mathbf{B}' \otimes \mathbf{B}^h) \\ \boldsymbol{\mathcal{N}}_V^R &= \mathbf{u}' \otimes \mathbf{u}' - \mathbf{B}' \otimes \mathbf{B}' \\ \boldsymbol{\mathcal{N}}_I^C &= -(\mathbf{u}^h \otimes \mathbf{B}' + \mathbf{u}' \otimes \mathbf{B}^h) \\ &\quad +(\mathbf{B}^h \otimes \mathbf{u}' + \mathbf{B}' \otimes \mathbf{u}^h) \\ \boldsymbol{\mathcal{N}}_I^R &= -\mathbf{u}' \otimes \mathbf{B}' + \mathbf{B}' \otimes \mathbf{u}'.\end{aligned} \tag{40}$$

To close the problem, we must still determine $\mathbf{U}'$. We recognize that Eq. (31) provides an equation that, in principle, can be solved for $\mathbf{U}'$. However, solving this equation is just as difficult as solving the full MHD equations. We can, however, obtain an approximation for $\mathbf{U}'$.[26] This is given by

$$\mathbf{U}' \approx -\mathbb{P}' \boldsymbol{\tau} \mathbb{P}'^T \mathcal{R}(\mathbf{U}^h). \tag{41}$$

In Eq. (41), $\tau$ is an algebraic approximation to the inverse differential operator. It represents an intrinsic grid time-scale. More specifically, it is a combination of advective and diffusive time-scales.[27–29] It is given as $\tau = \mathrm{diag}(\tau^V, \tau_c^V, \tau^I, \tau_c^I)$ with

$$\tau^V = \frac{1}{\sqrt{\frac{4}{h^2}\left((u^h_{\text{rms}})^2 + (B^h_{\text{rms}})^2\right) + 3\pi\left(\frac{4\nu}{h^2}\right)^2}}, \tag{42}$$

$$\tau^V_c = \frac{1}{\tau^V}\left(\frac{h}{6\sqrt{2}}\right)^2, \tag{43}$$

$$\tau^I = \frac{1}{\sqrt{\frac{4}{h^2}(B^h_{\text{rms}})^2 + 3\pi\left(\frac{4\nu}{h^2}\right)^2}}, \tag{44}$$

$$\tau^I_c = \frac{1}{\tau^I}\left(\frac{h}{6\sqrt{2}}\right)^2. \tag{45}$$

Here, the "rms" quantities are the root-mean square values averaged over the entire simulation volume. From Eq. (41), we conclude that the approximation to $\mathbf{U}'$ is driven by the residual of the coarse scales, $\mathcal{R}(\mathbf{U}^h)$,

$$\mathcal{R}(\mathbf{U}^h) = \begin{bmatrix} \dfrac{\partial \mathbf{u}^h}{\partial t} + \nabla\cdot\boldsymbol{\mathcal{N}}^h_V + \nabla P^h - \nu\nabla^2\mathbf{u}^h - \mathbf{f} \\ \nabla\cdot\mathbf{u}^h \\ \dfrac{\partial \mathbf{B}^h}{\partial t} + \nabla\cdot\boldsymbol{\mathcal{N}}^h_I + \nabla r^h - \eta\nabla^2\mathbf{B}^h - \mathbf{g} \\ \nabla\cdot\mathbf{B}^h \end{bmatrix}. \tag{46}$$

Note that in the above equation

$$\boldsymbol{\mathcal{N}}^h_V = \mathbf{u}^h\otimes\mathbf{u}^h - \mathbf{B}^h\otimes\mathbf{B}^h, \tag{47}$$

$$\boldsymbol{\mathcal{N}}^h_I = -\mathbf{u}^h\otimes\mathbf{B}^h + \mathbf{B}^h\otimes\mathbf{u}^h. \tag{48}$$

Using Eq. (46) in Eq. (41) and making use of the orthogonality between the function spaces $\boldsymbol{\mathcal{V}}^h$ and $\boldsymbol{\mathcal{V}}'$ yield

$$\mathbf{U}' \approx \begin{bmatrix} \mathbf{U}' \approx -\mathbb{P}'\boldsymbol{\tau}\mathbb{P}'^T\mathcal{R}(\mathbf{U}^h) \\ 0 \\ \mathbf{U}' \approx -\mathbb{P}'\boldsymbol{\tau}\mathbb{P}'^T\mathcal{R}(\mathbf{U}^h) \\ 0 \end{bmatrix}. \tag{49}$$

That is, the fine-scale contribution to the two pressure terms is zero. We note that this approximation for $\mathbf{U}'$ preserves a key feature of the equation for $\mathbf{U}'$ (Eq. (31)) in that if the coarse scale solution is exact, that is, $\mathcal{A}(\mathbf{W},\mathbf{U}^h) = (\mathbf{W},\mathbf{F}), \forall\,\mathbf{W}\in\boldsymbol{\mathcal{V}}$, then $\mathbf{U}' = 0$. Equivalently, if the residual of the coarse scales is zero, then the fine scales vanish. On the other hand, if the residual is not zero then the approximation to the fine scales is active and the effect of the fine scales is directly included in the equation for the coarse scales.

To summarize, the VMS leads to Eq. (38) for the resolved scales, where the unresolved scales are given by Eq. (41) (and, more specifically, with our selected basis functions, by Eq. (49)).

From Eq. (40), we conclude that the equation for the resolved scales includes subgrid stress contributions from the cross stresses and Reynolds stresses. It has been shown that the VMS is able to capture cross stress terms well but is a poor model for the Reynolds stress terms.[30] Motivated by this, in the present work, we will retain the VMS models that contribute to the cross stresses and drop the models that contribute to the Reynolds stresses. The VMS model is: *Find* $\mathbf{U}^h\in\boldsymbol{\mathcal{V}}^h$ *such that* $\forall\,\mathbf{W}^h\in\boldsymbol{\mathcal{V}}^h$,

$$\begin{aligned}\mathcal{A}(\mathbf{W}^h,\mathbf{U}^h) + (\mathbf{w}^h, \nabla\cdot\boldsymbol{\mathcal{N}}^C_V) \\ +(\mathbf{v}^h, \nabla\cdot\boldsymbol{\mathcal{N}}^C_I) = (\mathbf{W}^h,\mathbf{F}),\end{aligned} \tag{50}$$

where $\boldsymbol{\mathcal{N}}^C_V$ and $\boldsymbol{\mathcal{N}}^C_I$ are given by Eq. (40) and the fine scales $\mathbf{u}'$ and $\mathbf{B}'$ are given by Eq. (49). For flows in which either the Reynolds number or the magnetic Reynolds number (or both) are large, the Reynolds stresses will play a significant role. We will account for this by introducing an eddy viscosity model in Eq. (50) in Sec. III C.

We note that the VMS has been shown to be dissipative overall.[30] However, it does allow for the possibility of local backscatter which is associated with the inverse energy cascade that is known to occur in MHD.

### B. Residual-based EVM

We now return to the discussion of eddy viscosity models. The VMS provided us with an expression for the subgrid fields (Eq. (41)). With this expression, we propose a new, residual-based EVM of the form

$$\begin{aligned}\mathcal{M}(\mathbf{W}^h,\mathbf{U}^h;\mathbf{c},h) = (\nabla\mathbf{w}^h, 2\overline{C}_0 h|\mathbf{u}'|\nabla^s\mathbf{u}^h) \\ + (\nabla\mathbf{v}^h, 2\overline{C}_0 h|\mathbf{u}'|\mathbf{J}^h),\end{aligned} \tag{51}$$

where $\mathbf{u}'$ is given by Eq. (49). We observe that the eddy viscosity and magnetic diffusivity for this new model are

$$\nu_T = \eta_T = 2\overline{C}_0 h|\mathbf{u}'|, \tag{52}$$

which is motivated through a direct analogy with molecular viscosity. The turbulent eddy viscosity may be expressed as the product of a fluctuating velocity and a length scale (the mean free path). A similar analogy can be made for the turbulent magnetic diffusivity $\eta_T$ via the Drude model. This formulation has the benefit that it is residual-based and in that sense it is inherently dynamic. In particular, in regions where the flow is more-or-less laminar, the residual for the resolved scales is small, and as a result, the viscosity and the subgrid model automatically vanish. Based on this argument, we expect that the parameter $\overline{C}_0$ above has a chance at being a global parameter that does not have to be tuned from one region to another. For hydrodynamic turbulence, this parameter has been evaluated by equating the subgrid dissipation of the EVM to the total dissipation in the limit of an infinitely long inertial range.[31] Following a similar procedure (see the Appendix) for MHD and assuming that the total energy spectrum for incompressible MHD is

$$E^T(k) = C_K\epsilon^{2/3}k^{-5/3}, \tag{53}$$

where $C_K$ is the Kolmogorov constant for the total energy spectrum, we find

where

$$\overline{C}_0 = \overline{C}\alpha^{-1/2}, \tag{54}$$

$$\alpha = \frac{|\mathbf{u}'|^2}{|\mathbf{u}'|^2 + |\mathbf{B}'|^2}, \tag{55}$$

$$\overline{C} = \left(\frac{4}{27C_K^3\pi^2}\right)^{1/2}. \tag{56}$$

For $C_K = 2.2$ (Ref. 4), this yields $\overline{C} = 3.75 \times 10^{-2}$. Using the definition of $\overline{C}_0$ (Eq. (54)) in Eq. (51), we arrive at a new expression for the RBEVM

$$\mathcal{M}(\mathbf{W}^h, \mathbf{U}^h; \mathbf{c}, h) = (\nabla \mathbf{w}^h, 2\overline{C}h\sqrt{|\mathbf{u}'|^2 + |\mathbf{B}'|^2}\nabla^s \mathbf{u}^h) + (\nabla \mathbf{v}^h, 2\overline{C}h\sqrt{|\mathbf{u}'|^2 + |\mathbf{B}'|^2}\mathbf{J}^h). \tag{57}$$

We note that several estimates exist for $C_K$ in MHD turbulence[32] and the value of $\overline{C}$ depends on this choice. Further, the existence of a $k^{-5/3}$ inertial range in MHD is not a settled matter. In light of this, our value of $\overline{C}$ may be a candidate value among other possible values.

### C. Mixed model for MHD

Finally, we propose a mixed model for incompressible MHD in which the cross-stresses are modeled with the VMS and the Reynolds stresses are modeled with the new residual-based EVM. This method is: *Find* $\mathbf{U}^h \in \mathcal{V}^h$ *such that* $\forall\, \mathbf{W}^h \in \mathcal{V}^h$,

$$\mathcal{A}(\mathbf{W}^h, \mathbf{U}^h) + (\mathbf{w}^h, \nabla \cdot \boldsymbol{\mathcal{N}}_V^C) + (\mathbf{v}^h, \nabla \cdot \boldsymbol{\mathcal{N}}_I^C) + \mathcal{M}(\mathbf{W}^h, \mathbf{U}^h; \mathbf{c}, h) = (\mathbf{W}^h, \mathbf{F}), \tag{58}$$

where $\mathcal{M}(\cdot, \cdot; \cdot, \cdot)$ is given by Eq. (57). Equation (58) represents a consistent numerical formulation. In both the models for the cross stresses and Reynolds stresses, the approximation for the unresolved scales from the VMS is used. The cross-stress terms are represented by terms that are identical to the exact expressions; the only approximation is in the expression for the fine-scales. The Reynolds stresses are represented by eddy viscosity terms whose magnitude is proportional to the magnitude of the fine-scale fields. We note that the EVM that is used to account for the Reynolds stresses is entirely dissipative. However, the VMS portion still allows for the possibility of local backscatter.

### D. Summary

We have considered several LES models for the incompressible MHD equations. We now take the time to summarize them in a single equation. This equation, which is to be solved for $\mathbf{U}^h$, reads: *Find* $\mathbf{U}^h \in \mathcal{V}^h$ *such that* $\forall\, \mathbf{W}^h \in \mathcal{V}^h$,

$$\mathcal{A}(\mathbf{W}^h, \mathbf{U}^h) + (\mathbf{w}^h, \nabla \cdot \boldsymbol{\mathcal{N}}_V^C) + (\mathbf{v}^h, \nabla \cdot \boldsymbol{\mathcal{N}}_I^C) + (\nabla \mathbf{w}^h, 2\nu_T \nabla^s \mathbf{u}^h) + (\nabla \mathbf{v}^h, 2\eta_T \mathbf{J}^h) = (\mathbf{W}^h, \mathbf{F}), \tag{59}$$

where $\mathcal{A}(\mathbf{W}^h, \mathbf{U}^h)$ is given by Eq. (21) and contains all the terms present in a Galerkin approximation (no model). In addition,

1. For the Smagorinsky EVMs, $\boldsymbol{\mathcal{N}}_V^C = \boldsymbol{\mathcal{N}}_I^C = 0$ and $\nu_T$ and $\eta_T$ are given by

$$\nu_T = (C_V^S h)^2 \boldsymbol{\mathcal{S}}, \tag{60}$$

$$\eta_T = (C_I^S h)^2 |\mathbf{j}|. \tag{61}$$

   The parameters, $C_V^S$ and $C_I^S$, that appear in these equations are determined dynamically.
2. For the VMS model, $\nu_T = \eta_T = 0$ and expressions for the cross stress interactions $\boldsymbol{\mathcal{N}}_V^C$ and $\boldsymbol{\mathcal{N}}_I^C$ are provided in Eq. (40).
3. For the residual-based EVMs, $\boldsymbol{\mathcal{N}}_V^C = \boldsymbol{\mathcal{N}}_I^C = 0$ and $\nu_T$ and $\eta_T$ are given by

$$\nu_T = \eta_T = \overline{C}h\sqrt{|\mathbf{u}'|^2 + |\mathbf{B}'|^2}, \tag{62}$$

   where $\overline{C} = 3.75 \times 10^{-2}$. This constant has the potential to be a global parameter.
4. In the mixed model, both the eddy viscosity models and the VMS cross stress models are active. That is, no term in Eq. (59) is dropped. The turbulent eddy diffusivities, $\nu_T$ and $\eta_T$, are given by the same expressions as in the RBEVM (Eq. (62)).

Next, we test the performance of each of these models on a canonical turbulent MHD flow.

## IV. RESULTS

In this section, the performance of the models is assessed with a standard Taylor-Green flow generalized to MHD. The initial condition for the velocity field is[33]

$$\mathbf{u}(x, y, z, t = 0) = u_0 \begin{bmatrix} \sin(x)\cos(y)\cos(z) \\ -\cos(x)\sin(y)\cos(z) \\ 0 \end{bmatrix}. \tag{63}$$

A generalization to MHD considers an initial magnetic field of the form[34]

$$\mathbf{B}(x, y, z, t = 0) = B_0 \begin{bmatrix} \cos(x)\sin(y)\sin(z) \\ \sin(x)\cos(y)\sin(z) \\ -2\sin(x)\sin(y)\cos(z) \end{bmatrix}. \tag{64}$$

Initially, there is no cross helicity in this flow field, and this fact remains true for the duration of the simulation. All models, unless otherwise specified, are computed with $N = 32$ modes in each direction and are compared to a DNS run with $N = 512$. The domain is a periodic box of size $[-\pi, \pi]^3$. We define the Reynolds number $Re$ and magnetic Reynolds number $Rm$ as

$$Re = \frac{u_{\text{rms}} L^V}{\nu}, \tag{65}$$

$$Rm = \frac{u_{\text{rms}} L^M}{\eta}. \tag{66}$$

The characteristic length scales $L^V$ and $L^M$ are computed as

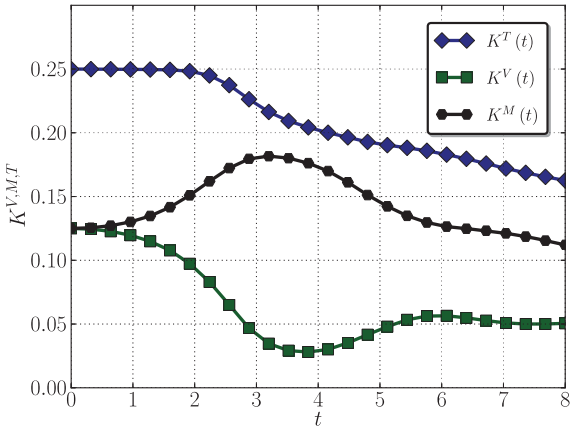


FIG. 1. Evolution of MHD energies for the decaying Taylor-Green vortex (DNS).

$$L^{V,M} = \frac{\int \frac{1}{k} E^{V,M}(k)\mathrm{d}k}{\int E^{V,M}(k)\mathrm{d}k}, \tag{67}$$

where $E^{V,M}(k)$ is the energy spectrum of the velocity field or the magnetic induction. The energy of each field is determined from their respective energy spectrum,

$$K^{T,V,M} = \int E^{T,V,M}(k)\,\mathrm{d}k, \tag{68}$$

where $K^{T,V,M}$ represents the total energy, velocity field energy, or magnetic induction energy at a certain time. The ratio of molecular viscosity to magnetic diffusivity, the magnetic Prandtl number ($Pr = Rm/Re$), is unity. The diffusivities are $\nu = \eta = 2.5 \times 10^{-4}$ which correspond to Reynolds numbers of $Re = Rm = 5.1 \times 10^3$. The initial velocity and magnetic fields are scaled so that the total energy, which is the sum of the kinetic and magnetic energies, is initially equal to 0.25. The initial state also has the kinetic and magnetic energies equal to each other. The evolution of the total energy, kinetic energy, and magnetic energy is presented in Fig. 1.

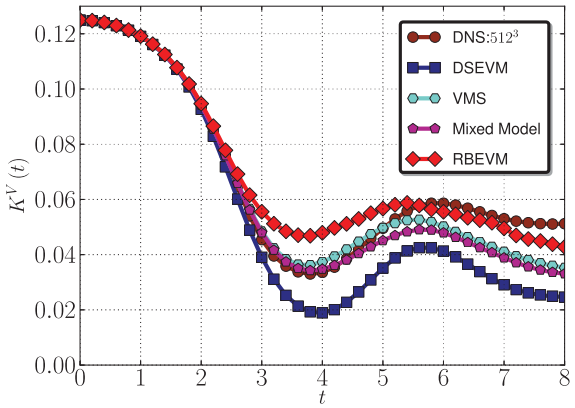


FIG. 2. Time evolution of kinetic energy as predicted by the LES models derived in this paper and compared to DNS.

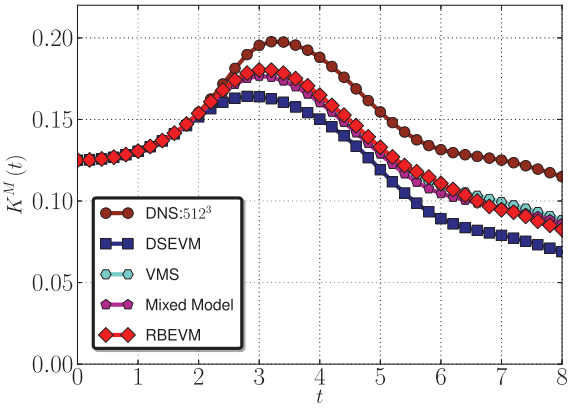


FIG. 3. Time evolution of magnetic energy as predicted by the LES models derived in this paper and compared to DNS.

We observe that although the total energy is decaying throughout the simulation the kinetic and magnetic energies can either gain or lose energy. This is a characteristic of MHD flows: one of the fields (here the magnetic field) gains energy at the expense of the other field (in this case, the velocity field). In Figs. 2 and 3, we present the evolution of the kinetic and magnetic energies, respectively, as predicted by each of the LES models derived in this paper. These figures indicate that the VMS and mixed models provide the best performance. However, all of the models presented in this paper appear to provide too much dissipation. In Secs. IV A–IV C, we discuss the performance of each of these models in more detail by considering their energy spectra.

### A. VMS

In Fig. 4, we compare the performance of the VMS model and the dynamic Smagorinsky model in predicting the total energy spectrum at $t = 8$. We observe that the DSEVM is overly dissipative for all wavenumbers, whereas the VMS model produces results that are very accurate in the mid-wavenumber range but overpredict the energy at wavenumbers near the cutoff. Based on these observations, it is fair to say that the DSEVM is too dissipative while the VMS model is not dissipative enough and that the latter is more accurate than the former.

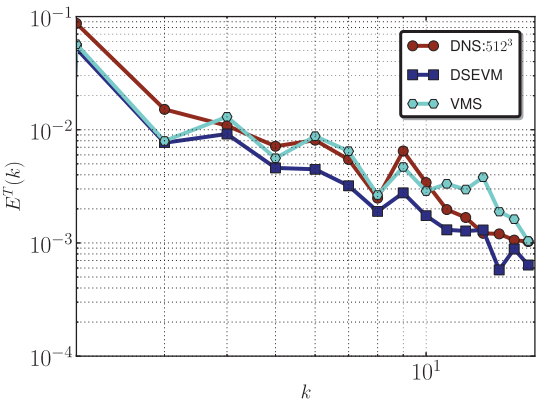


FIG. 4. Comparison of the VMS model and the dynamic Smagorinsky model. The energy spectrum of the total energy, $E^T(k)$, at $t = 8$ is presented.

A similar behavior for the VMS has been observed in the context of hydrodynamic turbulence.[29] This has been attributed to the fact that the VMS model is an accurate model for the cross-stresses and not for the Reynolds stresses. This has motivated us to consider the mixed model that employs the VMS model in conjunction with the residual based eddy viscosity model. In Sec. IV B, we first consider the RBEVM by itself and thereafter examine the performance of the mixed model.

### B. RBEVM

The RBEVM for MHD retains the consistency of the VMS model and the ability of the EVMs to capture the effects of the Reynolds stresses. By consistency, we imply that the eddy viscosity in this model vanishes when the coarse scale residual is equal to zero. In that case, the fine scales should be zero and we do not require a model to capture their effect. The RBEVM ensures that this happens. Fig. 5 assesses the performance of the RBEVM when compared to the standard DSEVM.

We observe that the performance of the two models is comparable although for large wavenumbers the RBEVM does not provide enough dissipation. Furthermore, the RBEVM is easier to implement as it does not require a dynamic procedure. Note, too, that the assumptions in deriving the constant $\overline{C}$ in the RBEVM formulation could be modified to better account for the energy spectrum behavior in the inertial range. Unfortunately, not knowing, this behavior *a priori* would require some *ad-hoc* methods (or even a dynamic procedure) for determining $\overline{C}$, which we wish to avoid.

### C. Mixed model

In Fig. 6, we assess the performance of the DSEVM, the VMS, and the mixed model. Note that the mixed model is a combination of the VMS and the RBEVM and since both of these models are consistent (they vanish when the coarse scales are accurate), the mixed model is also consistent. We observe that the mixed model is the most accurate. It appears to have retained the accuracy of the VMS model in the mid wavenumber range and slightly improved on it in the high wavenumber range through enhanced dissipation. This is also observed in the plots for the velocity and magnetic spectra in Figs. 7 and 8, respectively. In both of these plots, the mixed model is the most accurate followed by the VMS model and the DSEVM.

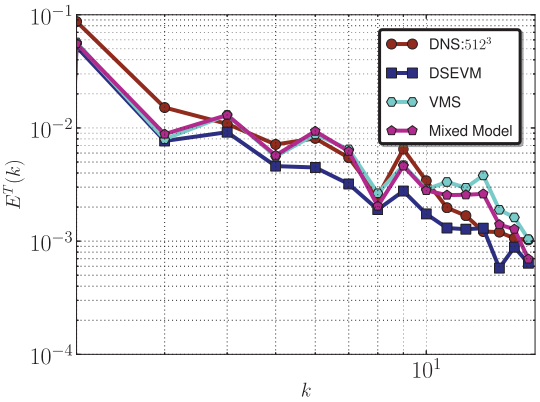


FIG. 6. The total energy spectrum at $t = 8$ for LES models (DSEVM, VMS, MM) compared to the DNS simulation.

We note that at the Reynolds number considered in this simulation, the difference between the VMS and the mixed model is not especially significant. This implies that within the mixed model the contribution from the RBEVM component is not very large. We can understand this by recognizing that the Reynolds number for the flow is not high and so we do not anticipate the Reynolds stresses (which is what the RBEVM represents) to play a significant role. One way to test this explanation is to consider a higher Reynolds number.

Fig. 9 presents the time-evolution of the energy ratio between the magnetic and velocity fields ($K^M/K^V$) for a flow field with $\nu = \eta = 6.25 \times 10^{-5}$ ($Re = Rm = 2.1 \times 10^4$). All other parameters are the same as in the previous problem. The DNS is obtained from a simulation by Pouquet *et al.* and is computed with N = 2048 modes in each direction. Qualitatively, it appears that the mixed model performs best overall. Near the peak of dissipation ($\sim t = 3.90$), it is in best agreement with the DNS data.

To gain further insight, we compare the compensated total energy spectrum averaged around the peak of total

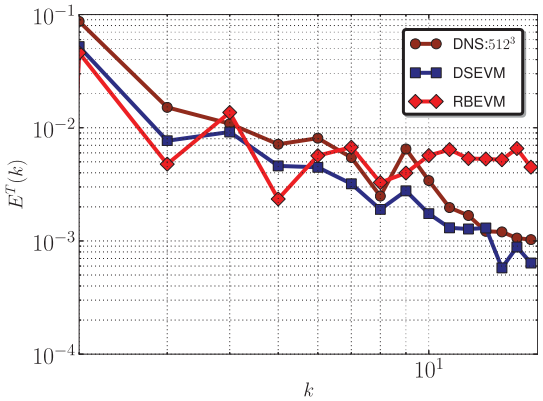


FIG. 5. A comparison of the total energy spectra of two EVMs: the standard dynamic Smagorinsky EVM and the new residual-based EVM.

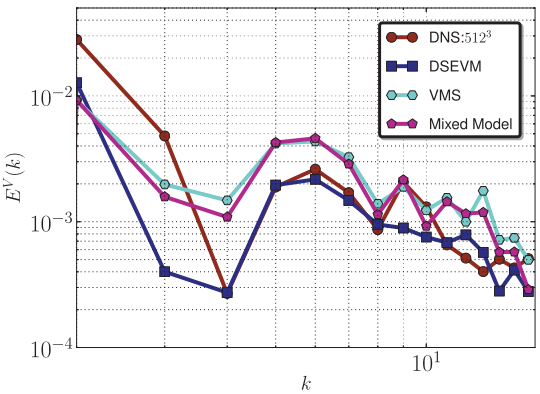


FIG. 7. The velocity energy spectrum at $t = 8$ for LES models (DSEVM, VMS, MM) compared to the DNS simulation.

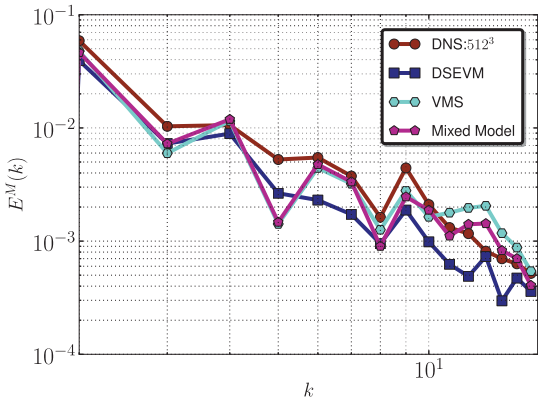


FIG. 8. The magnetic energy spectrum at $t=8$ for LES models (DSEVM, VMS, MM) compared to the DNS simulation.

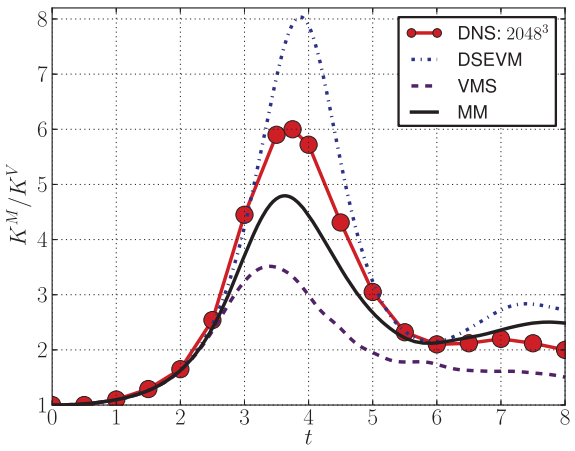


FIG. 9. Time-evolution of energy ratio, $K^M/K^V$ for the decaying Taylor-Green vortex with $Re = Rm = 2.1 \times 10^4$. DNS results are from a previous work.[35]

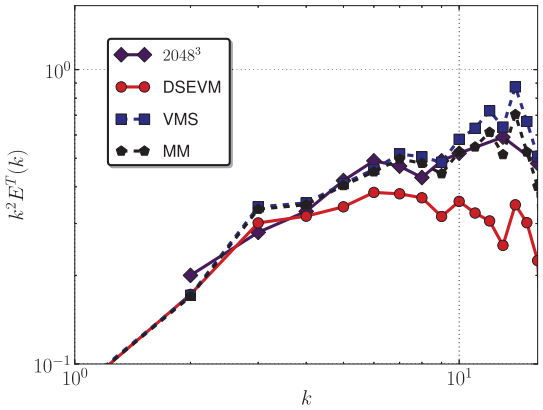


FIG. 10. Compensated total energy spectra, averaged about peak of total dissipation, for the run with $Re = Rm = 2.1 \times 10^4$. DNS results are from a previous work.[35]

dissipation ($t \in [3.5, 5]$) for each of the models with the DNS data.[35] In Fig. 10, the advantages of the mixed model become apparent; the mixed model is in very good agreement with the DNS simulation, while the VMS is underdiffuse in the high wavenumbers and the DSEVM provides far too much dissipation overall.

We note that previous work has suggested that the ratio of the dissipation from the Reynolds stresses to the total turbulent dissipation is approximately 1/3.[36] This would imply that it is necessary to replace $\overline{C}$ with $\overline{C}/3$ in Eq. (57) for the mixed model. We tested this modification for the decaying Taylor-Green vortex but found that leaving the dissipation constant $\overline{C}$ alone gives the best results. By using $\overline{C}/3$, the mixed model still represents an improvement over the VMS model, but this improvement is harder to discern.

## V. CONCLUSIONS AND FUTURE WORK

We have developed novel LES turbulence models for incompressible MHD. These models are

- A model based on the variational multiscale formulation
- A new residual-based EVM
- A mixed model that combines the first two

All these models are driven by the residual of the coarse scale variables and hence vanish when the coarse scales are accurate. In this sense, they are consistent. Because of this feature, we also anticipate that the parameters appearing in these models do not have to be adapted or evaluated dynamically. Indeed, in the simulations presented in this paper, they were held fixed.

These models were tested using a decaying Taylor-Green vortex with $Re = Rm = 5.1 \times 10^3$. They were compared to the classic dynamic Smagorinsky EVM as well as results from a DNS simulation with 512 modes in each direction. We found that at these Reynolds numbers, the mixed model provides the best results followed by the VMS model. The RBEVM and the DSEVM produced results that were the least accurate.

A greater distinction between the performances of the models was seen upon considering a higher Reynolds number flow. The DNS data for a high Reynolds number flow was taken from a simulation that was run with 2048 modes in each direction.[35] The LES was run with only 32 modes in each direction. The ratio of the number of modes in the DNS to the LES simulations in this case is 262:144. Even at this large ratio, the new mixed model performed exceptionally well.

Although the new models for incompressible MHD (in particular, the mixed model) yielded good results, there might be some room for improvement. In particular, the subgrid stresses in the momentum equation involve the subgrid velocity fluctuations *and* the subgrid magnetic fluctuations. However, the eddy viscosity model that we employed was designed specifically for the subgrid velocity fluctuations. It did not contain a term whose goal was to model the subgrid Maxwell stresses.

Additional studies are planned that will compare our new models to more state-of-the art models such as an alignment-based eddy viscosity model.[9] We also intend to explore the abilities of the new models to represent interesting and important MHD phenomena such as alignment of the velocity and magnetic field, the effects of magnetic helicity, and the inverse cascade of magnetic helicity. We have already demonstrated the ability of the VMS model to reproduce the subgrid

dynamo effect under certain physical conditions. In a future work, we plan to systematically demonstrate this phenomenon with numerical experiments.

There are several extensions of this work that are intriguing. For example, it would be interesting to perform a simulation of the solar wind using the new mixed model. In this case, rather than compare with DNS simulations, the data are available.[37–39] that will allow us to assess the performance of the new LES models on a realistic problem for which experimental results exist. The ability to accurately simulate and thereby predict solar wind activity is important in forecasting space weather in the vicinity of our planet.

Furthermore, rather than focus on problems with periodic boundary conditions, it will be worthwhile to consider problems with more realistic boundary conditions and boundary layers. A relatively straightforward problem to consider initially is the turbulent MHD channel flow problem. This analog to channel flow in fluid dynamics will introduce a turbulent boundary layer whose characteristics will change depending on the relative importance of the magnetic and velocity fields.

## ACKNOWLEDGMENTS

This research is supported in part by the Department of Energy Office of Science Graduate Fellowship Program (DOE SCGF), made possible in part by the American Recovery and Reinvestment Act of 2009, administered by ORISE-ORAU under Contract No. DE-AC05-06OR23100. Also the support of the SUR Blue Gene at Rensselaer Polytechnic Institute for the DNS calculation is gratefully acknowledged. The senior author would like to acknowledge the support of Erasmus Mundus Master Course Lectureship at Universidad Politécnica de Cataluña and the Humboldt Foundation award for experienced researchers.

## APPENDIX: DERIVATION OF THE RBEVM CONSTANT

We now proceed with a derivation of the calibration constant $\overline{C}$ in the RBEVM. The rate of dissipation of the total energy for incompressible MHD with the RBEV model is

$$\epsilon^h = 2\langle \nu_T \mathbf{S}^h : \mathbf{S}^h + \eta_T \mathbf{J}^h : \mathbf{J}^h \rangle, \tag{A1}$$

where we have neglected the contribution from molecular viscosity and magnetic diffusivity. With $\nu_T = \eta_T = \overline{C}_0 h |\mathbf{u}'|$,

$$\epsilon^h = 2\overline{C}_0 h \langle |\mathbf{u}'| (\mathbf{S}^h : \mathbf{S}^h + \mathbf{J}^h : \mathbf{J}^h) \rangle, \tag{A2}$$

$$\approx 2\overline{C}_0 h \langle |\mathbf{u}'|^2 \rangle^{1/2} \langle \mathbf{S}^h : \mathbf{S}^h + \mathbf{J}^h : \mathbf{J}^h \rangle. \tag{A3}$$

We would like to express each term on the right-hand-side of Eq. (A3) in terms of the total energy spectrum. To do this, we assume that the spectra for $\mathbf{u}$ and $\mathbf{B}$ differ by a multiplicative constant so that we may replace $|\mathbf{u}'|^2$ with $\alpha(|\mathbf{u}'|^2 + |\mathbf{B}'|^2)$ where

$$\alpha = \frac{|\mathbf{u}'|^2}{|\mathbf{u}'|^2 + |\mathbf{B}'|^2}. \tag{A4}$$

Using this in Eq. (A3), we arrive at

$$\epsilon^h \approx 2\overline{C}_0 h \left( 2\alpha \int_{k^h}^{\beta k^h} E^T(k)\, \mathrm{d}k \right)^{1/2} \times \left( \int_0^{k^h} k^2 E^T(k)\, \mathrm{d}k \right). \tag{A5}$$

We assume a power law for the total energy spectrum,

$$E^T(k) = C_K C' \epsilon^m k^n, \tag{A6}$$

where $C_K$ is a dimensionless constant and $\epsilon$ is the exact dissipation rate. The parameter $C'$ depends on the physics of the problem. Note that $C'$ is not a constant but a dimensional parameter. After some algebra, we obtain

$$\epsilon^h \approx \overline{C}_0 2\sqrt{2} h \sqrt{\alpha} (C_K C')^{3/2} \frac{(k^h)^{1/2\,(3n+7)}}{(n+3)(n+1)^{1/2}} \times (\beta^{n+1} - 1)^{1/2} \epsilon^{3m/2}. \tag{A7}$$

Equating the modeled and exact dissipation rate, $\epsilon^h = \epsilon$, we arrive at

$$\overline{C}_0 = \overline{C} \alpha^{-1/2}, \tag{A8}$$

where

$$\overline{C} = \frac{1}{2\sqrt{2} h (C_K C')^{3/2} K (\beta^{n+1} - 1)^{1/2} \epsilon^{(3m-2)/2}}, \tag{A9}$$

with

$$K = \frac{(k^h)^{1/2(3n+7)}}{(n+3)(n+1)^{1/2}}. \tag{A10}$$

Note that, in general, the calibration constant $\overline{C}$ will not be problem independent as it has a dependency on the dissipation rate. However, if we assume a Kolmogorov spectrum ($m = 2/3$, $n = -5/3$, $C_K = 2.2$, $C' = 1$) and recall that the cutoff wavenumber is $k^h = \pi/h$ and furthermore take $\beta \to \infty$ (to account for all of the subgrid scales), we have

$$\overline{C} = \left( \frac{4}{27} \right)^{1/2} \frac{1}{C_K^{3/2} \pi}. \tag{A11}$$

Returning now to the expressions for the eddy viscosity and the magnetic diffusivity, we have

$$\begin{aligned} \nu_T = \eta_T &= \overline{C}_0 h |\mathbf{u}'| \\ &= \overline{C} \alpha^{-1/2} h |\mathbf{u}'| \\ &= \overline{C} h (\sqrt{|\mathbf{u}'|^2 + |\mathbf{B}'|^2}). \end{aligned} \tag{A12}$$

[1]R. Moreau, *Magnetohydrodynamics* (Springer, 1990), Vol. 3.
[2]P. Davidson, *An Introduction to Magnetohydrodynamics* (Cambridge University Press, 2001), Vol. 25.
[3]U. Müller and L. Bühler, *Magnetofluiddynamics in Channels and Containers* (Springer-Verlag, 2001).
[4]D. Biskamp, *Magnetohydrodynamic Turbulence* (Cambridge University Press, 2003).

[5]H. Goedbloed, S. Poedts, and E. Zita, "Principles of magnetohydrodynamics," Am. J. Phys. **74**, 462 (2006).
[6]M. Theobald, P. Fox, and S. Sofia, "A subgrid-scale resistivity for magnetohydrodynamics," Phys. Plasmas **1**, 3016 (1994).
[7]N. Haugen and A. Brandenburg, "Hydrodynamic and hydromagnetic energy spectra from large eddy simulations," Phys. Fluids **18**, 075106 (2006).
[8]A. Yoshizawa, "Subgrid-scale modeling of magnetohydrodynamic turbulence," J. Phys. Soc. Jpn. **60**, 9–12 (1991).
[9]W. Muller and D. Carati, "Large-eddy simulation of magnetohydrodynamic turbulence," Comput. Phys. Commun. **147**, 544–547 (2002).
[10]M. Germano, U. Piomelli, P. Moin, and W. Cabot, "A dynamic subgrid-scale eddy viscosity model," Phys. Fluids A **3**, 1760 (1991).
[11]V. John and A. Kindl, "Variants of projection-based finite element variational multiscale methods for the simulation of turbulent flows," Int. J. Numer. Methods Fluids **56**, 1321–1328 (2008).
[12]A. Vreman, "An eddy-viscosity subgrid-scale model for turbulent shear flow: Algebraic theory and applications," Phys. Fluids **16**, 3670 (2004).
[13]Y. Ponty, H. Politano, and J. Pinton, "Simulation of induction at low magnetic Prandtl number," Phys. Rev. Lett. **92**, 144503 (2004).
[14]B. Knaepen and P. Moin, "Large-eddy simulation of conductive flows at low magnetic Reynolds number," Phys. Fluids **16**, 1255 (2004).
[15]S. Orszag, in *Fluid dynamics: Les Houches Summer School, 1973*, edited by R. Balian and J. Peube (Gordon and Breach, 1977).
[16]J. Baerenzung, H. Politano, Y. Ponty, and A. Pouquet, "Spectral modeling of turbulent flows and the role of helicity," Phys. Rev. E **77**, 046303 (2008).
[17]J. Baerenzung, H. Politano, Y. Ponty, and A. Pouquet, "Spectral modeling of magnetohydrodynamic turbulent flows," Phys. Rev. E **78**, 026310 (2008).
[18]D. Holm, "Fluctuation effects on 3D Lagrangian mean and Eulerian mean fluid motion," Physica D **133**, 215–269 (1999).
[19]D. C. Montgomery and A. Pouquet, "An alternative interpretation for the Holm alpha model," Phys. Fluids **14**, 3365–3366 (2002).
[20]D. Holm, "Taylors hypothesis, Hamiltons principle, and the Lans-$\alpha$ model for computing turbulence," Los Alamos Sci. **29**, 172 (2005).
[21]D. Holm, "Lagrangian averages, averaged Lagrangians, and the mean effects of fluctuations in fluid dynamics," Chaos **12**, 518–530 (2002).
[22]J. Shadid, R. Pawlowski, J. Banks, L. Chacon, P. Lin, and R. Tuminaro, "Towards a scalable fully-implicit fully-coupled resistive MHD formulation with stabilized FE methods," J. Comput. Phys. **229**, 7649–7671 (2010).
[23]R. Codina, "Stabilized finite element approximation of transient incompressible flows using orthogonal subscales," Comput. Methods Appl. Mech. Eng. **191**, 4295–4321 (2002).
[24]T. Hughes, L. Franca, and G. Hulbert, "A new finite element formulation for computational fluid dynamics: VIII. The Galerkin/least-squares method for advective-diffusive equations* 1," Comput. Methods Appl. Mech. Eng. **73**, 173–189 (1989).
[25]T. Hughes, "Multiscale phenomena: Green's functions, the Dirichlet-to-Neumann formulation, subgrid scale models, bubbles and the origins of stabilized methods," Comput. Methods Appl. Mech. Eng. **127**, 387–401 (1995).
[26]Y. Bazilevs, V. Calo, J. Cottrell, T. Hughes, A. Reali, and G. Scovazzi, "Variational multiscale residual-based turbulence modeling for large eddy simulation of incompressible flows," Comput. Methods Appl. Mech. Eng. **197**, 173–201 (2007).
[27]F. Shakib, T. Hughes, and Z. Johan, "A new finite element formulation for computational fluid dynamics: X. The compressible Euler and Navier-Stokes equations," Comput. Methods Appl. Mech. Eng. **89**, 141–219 (1991).
[28]R. Codina and N. Hernández-Silva, "Stabilized finite element approximation of the stationary magneto-hydrodynamics equations," Comput. Mech. **38**, 344–355 (2006).
[29]Z. Wang and A. Oberai, "A mixed large eddy simulation model based on the residual-based variational multiscale formulation," Phys. Fluids **22**, 075107 (2010).
[30]Z. Wang and A. Oberai, "Spectral analysis of the dissipation of the residual-based variational multiscale method," Comput. Methods Appl. Mech. Eng. **199**, 810–818 (2010).
[31]A. Oberai, J. Lui, D. Sondak, and T. Hughes, "A residual-based eddy viscosity model for the LES of turbulent flows," Phys. Fluids (In revision).
[32]A. Beresnyak, "Spectral slope and Kolmogorov constant of MHD turbulence," Phys. Rev. Lett. **106**, 75001 (2011).
[33]M. Brachet, D. Meiron, S. Orszag, B. Nickel, R. Morf, and U. Frisch, "Small-scale structure of the Taylor-Green vortex," J. Fluid Mech. **130**, 411–452 (1983).
[34]E. Lee, M. Brachet, A. Pouquet, P. Mininni, and D. Rosenberg, "Lack of universality in decaying magnetohydrodynamic turbulence," Phys. Rev. E **81**, 016318 (2010).
[35]A. Pouquet, E. Lee, M. Brachet, P. Mininni, and D. Rosenberg, "The dynamics of unforced turbulence at high Reynolds number for Taylor–Green vortices generalized to MHD," Geophys. Astrophys. Fluid Dyn. **104**, 115–134 (2010).
[36]R. Kraichnan, "Eddy viscosity in two and three dimensions," J. Atmos. Sci. **33**, 1521–1536 (1976).
[37]M. Acuna, K. Ogilvie, D. Baker, S. Curtis, D. Fairfield, and W. Mish, "The global geospace science program and its investigations," Space Sci. Rev. **71**, 5–21 (1995).
[38]K. Ogilvie and M. Desch, "The wind spacecraft and its early scientific results," Adv. Space Res. **20**, 559–568 (1997).
[39]J. Podesta and J. Borovsky, "Scale invariance of normalized cross-helicity throughout the inertial range of solar wind turbulence," Phys. Plasmas **17**, 112905 (2010).